Optics and Lasers in Engineering 181 (2024) 108395

Contents lists available at ScienceDirect

Optics and Lasers in Engineering

journal homepage: www.elsevier.com/locate/optlaseng

Discernment of textile fibers by polarization-sensitive Digital Holographic microscope and machine learning

M. Valentino [a,b,1], J. Behal [a,c,1], C. Tonetti [d], R.A. Carletto [d], S. Itri [a], P. Memmolo [a], E. Stella [e], L. Miccio [a], V. Bianco [a,*], P. Ferraro [a]

[a] Institute of Applied Sciences and Intelligent Systems "E. Caianiello", National Research Council (ISASI-CNR), via Campi Flegrei 34, 80078 Pozzuoli, Napoli, Italy
[b] Department of Electrical Engineering and Information Technologies (DIETI), University of Naples "Federico II", via Claudio 21, 80125 Napoli, Italy
[c] Department of Optics, Faculty of Science, Palacky University, 17. listopadu 12, 77146 Olomouc, Czechia
[d] Institute of Intelligent Industrial Technologies and Systems for Advanced Manufacturing, National Research Council (STIIMA-CNR), Corso G. Pella 16, 13900 Biella, Italy
[e] Institute of Intelligent Industrial Technologies and Systems for Advanced Manufacturing, National Research Council (STIIMA-CNR), Via Giovanni Amendola, 122 D/O, 70126 Bari, Italy

ARTICLE INFO

Keywords:
Polarization-sensitive digital holography
Jones matrix
Birefringence
Machine learning
Classification
Textile animal fibers

ABSTRACT

Garment quality and preciousness depend on the type of textile fiber used in the manufacturing. The softer and rarer the animal fiber, the more expensive the textile garment. The cheapest clothes are made by mixing precious fibers such as cashmere with common ones such as sheep wool. To stop clothing counterfeit and quality forgery, checking the type of animal fibers used in textile industries is pivotal. More in general, law regulations require that the declared composition of a tissue meet some standards of quality that have to be assayed carefully by expert operators. Microscopy techniques such as Scanning Electron Microscopy (SEM) and Light Microscopy (LM) are commonly used to discriminate between textile animal fibers. However, analysis by SEM and LM depends on skilled experts called to judge, one-by-one, each fiber. This process is slow, cumbersome, and may be inaccurate, especially if the textile fibers share similar morphologies. Furthermore, the chemical treatments required by some textile processes can heavily modify the morphology of the fibers making more difficult to get correct results. In this work, the textile animal fibers are characterized by a polarization-sensitive, stain-free, Digital Holographic Microscopy (DHM) technique. In particular, we show how cashmere and wool fibers differ according to their anisotropy properties, e.g., birefringence. The optical characterization of textile fibers through the Jones matrix formalism allowed us extracting polarization-dependent DH features capable of accurately classifying three types of animal microfibers using a machine learning approach. Such promising results smooth the path towards an automatic, rapid, and objective identification process for textile industry and standardization purposes.

1. Introduction

Animal fibers are commonly used in textile industry for clothing production. Usually, most of garments are made of wool yarn or of sheep breeds yarn because of some morphological properties, such as the tiny scale of the fiber. Wool scales promote heat retention, moisture absorption and feltability [1,2]. The type and the rarity of animal fiber indicates the garment preciousness and authenticity.

For instance, cashmere, mohair, camelid fibers are considered top-quality fibers, while wool is less rare and precious [3,4]. Cashmere is a luxury animal fiber due to its rarity and softness, whose market is considered the top-level in the textile sector [5].

In some cases, to lower the production and in turn the selling costs, cashmere is mixed with sheep wool or other poorer quality fibers, altering the quality and the pureness of the garment and fueling the fraudulent market. However, the correct percentage composition of a textile product should be determined and declared by the producer and sellers.

Therefore, the discernment between cashmere and other animal fibers like fine wool is an important task for the textile production

* Corresponding author.
E-mail address: vittorio.bianco@isasi.cnr.it (V. Bianco).
[1] M.Valentino and J. Běhal equally contributed to the present manuscript.

https://doi.org/10.1016/j.optlaseng.2024.108395
Received 11 July 2023; Received in revised form 15 May 2024; Accepted 11 June 2024
Available online 2 July 2024

industry with strong influences on the market [6,7].

According to a report by the Organization for Economic Co-operation and Development (OECD) and the European Union Intellectual Property Office (EUIPO), counterfeit and pirated goods, including textiles, accounted for up to 3.3 % of global trade in 2016 [8]. This amounted to an estimated value of $509 billion USD, with the textile and apparel industry being one of the most affected sectors. The report also highlighted that the value of counterfeit textile and apparel products seized by customs authorities increased by 80 % between 2008 and 2016, indicating the growing prevalence of counterfeit textiles in the global market. Hence, we believe that developing new methods to automatically judge cashmere pureness is essential for safeguarding consumer interests, protecting economic interests, fostering innovation, ensuring legal compliance, and promoting environmental and social responsibility within the cashmere industry and beyond.

Moreover, from a circular economy perspective and taking into account that another source of fibers waste is represented by unwanted clothes and end-of-life textile products in the textile supply chain, it would be important to be able to recycle them. In this case, sorting is a fundamental step to separate and recycle textile materials correctly, on the basis of their fibers composition [9].

Based on that, methods to differentiate different type of fibers, in particular the animal hair fibers from each other are important to guarantee garment quality and adherence to standards.

Usually, thickness or diameter characterize natural and animal fibers. The high ratio between the length and the diameter of a fiber is a peculiarity of the final manufacturing product [2]. The smaller the diameter of a fiber, the more precious the fiber. Cashmere and Merino wool diameters measure about 10–18 μm [10], while coarse wool diameters measure more than 20 μm [7].

However, cashmere and wool share similarities in their external shape, and the characteristic diameters may vary significantly from the nominal ones. Thus, relying on the sole morphological characterization is not always the most reliable approach.

As we anticipated previously, fiber scales are pivotal to discriminate animal fibers, like cashmere and wool. Wool surface roughness, which differs on the basis of the typical cuticle scales of animal fibers, is used to differentiate wool fibers from other natural and synthetic ones [1,2]. There are different scale patterns, such as mosaic, petal, chevron, which can help in discrimination.

However, the manufacturing process can modify the scale layer of a fiber. Therefore, the sole roughness evaluation could be misleading in identifying fiber types. Microscopy methodologies are mostly used in this field.

The traditional microscopic methods to identify animal fibers, such as Scanning Electron Microscopy (SEM) and Light Microscopy (LM), involves the evaluation of the scale patterns, the diameters, the profile of the fiber, the scale thickness, and the frequency of the scales of the fibers [11,12].

LM is considered as the primary method due to its accessibility and affordability, and allows observing fiber morphology, fiber surface roughness, and fiber inner structure (shape, pigmentation and medullation) [13,14]. SEM permits the analysis of scale patterns and in particular of the cuticle's cells [12,15-17], especially in discerning wool and cashmere fibers [18]. Wortmann et al. identified wool contamination in cashmere with SEM analysis [19,20].

Despite the widespread use of LM and SEM methodologies, some limitations are evident. For instance, LM and SEM can suffer from operator dependence, long times of analysis, and fiber morphology impact (e.g. fibers with similar morphology or damaged can influence the classification accuracy).

Moreover, Transmission Electron Microscope (TEM) detected some blends of fibers with wool [4], different in scale heights. Atomic force microscopy was used to study the morphological roughness variations between treated and untreated cashmere fibers [21].

Another discriminative characteristic is the presence of calcium oxalate crystals on some animal fibers. Indeed, sheep breeds usually get in touch with plants present in their natural environment, which may release crystals on their coat [22]. Polarized light microscopy (PLM) distinguished wool, cotton and silk fibers from textile bast fibers thanks to the fibrillary orientation of calcium oxalate crystals [22]. More in general, PLM is a powerful instrument in detecting anisotropic fibers.

However, the discrimination of animal hair fibers by means of unaided microscopy observation is laborious and time consuming, as fibers have to be identified one by one relying on the operator expertise and skills.

To assess the composition of a mixture, the standard requires that at least 1000 fibers shall be examined for each sample and 100 measurements of fibers diameter made for each fiber type [23,24]. This procedure can take several days of an expert's work. Visual identification suffers from lack of automatization, and sometimes accuracy. When fibers share similar characteristic traits, morphology and surface roughness or when the fiber morphological characteristics are modified by textile processing, the correct identification becomes more difficult. Besides, in all the cases of visual analysis, the operator fatigue has to be considered, which reduces the identification accuracy after several hours of continuous work. For this reason, the procedure of microscopy observation for a garment has to be split into various shorter identification sessions, which further dilates the times for the quality assessment.

Monoclonal techniques, protein and lipids analysis methods, methods based on molecular markers [21,25-29] have been used to improve the quality of differentiation of textile fibers. For instance, the keratin extracted from cashmere, yak and wool, analyzed by liquid chromatography coupled with electrospray mass spectrometry (LC/ESI-MS) after digestion with trypsin, shows peptidic markers specific for each fiber [28,30]. This method resulted useful to assess garments quality, having high specificity and sensitivity and showing high level of reliability and in the quantification of cashmere, yak and wool fibers [28-30].

The proteomic analyses have a limit of fiber detection around 5 % [31], which is a good result. However, it is not reliable in identifying fibers in similar hybridized species [11].

Moreover, differential scanning calorimetry (DSC) was used to study the thermal behavior of animal fibers, in particular to distinguish cashmere from cheaper fibers (e.g., yak and wool) [32]. The discrimination among these fibers by DSC is possible only at qualitative level and only for pure sample, not for blends. Moreover, the textile industrial treatments modify fiber DCS traces, negatively influencing the results of the analysis [32].

Regarding the chemical characterization of microscopic samples, spectroscopy is the most suitable and reliable methodology [33]. Fourier Transform Infrared Spectroscopy (FTIR) offers a non-destructive method for identifying chemical compositions and structural features of fibers based on their vibrational spectra [34]. FTIR identified the different composition of amino acids contained in the keratin proteins of animal fibers, e.g. cashmere and wool [34]. The intensity of FTIR spectra of cashmere fibers differs from wool fibers spectra, and also cashmere of different origins has shown non-negligible spectral variations. Furthermore, the infrared spectral (IRS) analysis examined the major absorption intensity peaks of wool and acrylic fibers [35].

Recent advancements in spectroscopic techniques, such as Raman spectroscopy and Near-Infrared Spectroscopy (NIRS), offer rapid and accurate analysis of fiber properties, including fiber type, moisture content, and fiber blend ratios [36,37]. Sun et al. tested NIR on real market samples and achieved an accuracy of 93.33 % for cashmere textiles and 96.60 % for cashmere–wool blended textiles [37].

Using NIRS was used to extract several features, e.g., the mean and the standard deviation of fiber diameter and curvature, to assess the quality of alpaca fibers [38].

A random forest classification identified different textile fibers (wool, polyamide and silk) using the reflectance-FT-IR (r-FT-IR) spectra

[39].

However, spectroscopy methodologies often entail costly instrumentation, are time-consuming in calibration steps and can suffer from interference by the surrounding environment.

Besides, these methods require special preparation of the sample and are not applicable in case of different animal fibers blends, because they have very similar chemical characteristics showing identical spectra.

Here, an alternative, all-optical, approach is presented to classify cashmere and fine wool fibers. We use a custom-built polarization-sensitive Digital Holographic (DH) microscope to characterize the animal fibers in a stain-free manner, i.e., avoiding dyes and chemical treatments. DH [40] is a Quantitative Phase Imaging (QPI) technique that provides morphometrical information of the specimen [41]. The coherent light used in the DH optical system is modulated by the probed sample. After passing through the object, the phase of the complex field carries object information, being a function of the thickness and refractive index of the object. The DH microscope records a hologram, i.e., a pattern of sample-modulated fringes, that undergoes a numerical reconstruction process to gather the object complex amplitude [38]. This can be refocused in post-processing and provides two information channels, i.e., the amplitude and the phase-contrast maps of the object in sharp focus [41]. Introducing sensitivity to the polarization of light allows adding new information channels in space-multiplexed fashion. Especially, polarization-sensitive DH allows quantifying polarization changes induced by the object [42,43].

In this context, the birefringence-related information can contribute to discriminate microfibers [44,45]. In particular, synthetic and natural microfibers have been distinguished by using the polarization-sensitive DH system [46,47].

Behal et al. characterized in depth the polarimetric patterns of natural and synthetic microfibers adopting the Jones matrix formalism and used all-optical polarization-based features for classification purposes [46]. Specifically, the use of the Jones formalism enabled the full analysis of parameters associated to the object-dependent Jones matrix eigenmodes. In addition, Valentino et al. adopted a machine learning pipeline to identify each synthetic and natural microfiber in a polarization-sensitive DH flow-cytometer system [47].

In this work, we use the polarization-sensitive DH (PS-DH) microscope and measure all-optical features that characterize the animal fibers, i.e., morphological, refractive index variations, Jones features and other polarization-sensitive DH information channels (e.g. birefringence) to classify cashmere and wool fibers. This additional information can aid in more accurate discrimination of fibers compared to both LM and SEM. PS-DH does not require staining or labeling of fibers. This preserves the natural characteristics of fibers and eliminates the need for additional sample preparation steps. PS-DH has the potential to provide higher throughput imaging compared to SEM, which often involves time-consuming sample preparation and imaging procedures. Furthermore, PS-DH can capture large-area images in a single acquisition, enabling rapid screening and simultaneous analysis of multiple fibers. Our approach is aimed at developing an automatized identification process that could be used in textile industry and could facilitate the lab analysis during quality assays. The combination of polarization-sensitive DH system and machine learning is proved to furnish accurate classification, which paves the way to the objective and rapid discrimination of animal hair fibers disengaged from the skills and the unaided meticulous labor of experienced operators. It is worth pointing out that compact polarization-resolved holographic microscopes exist [48]. In the next future, such intelligent technology could be embedded in production lines for in situ quality inspections in textile industry.

2. Materials and methods

2.1. Experimental setup

Recently, we developed a polarization-sensitive DH microscope in transmission (Fig. 1) [46,47]. Here, the linearly polarized laser beam (Sapphire, SF, wavelength λ=532 nm) is spatially filtered, collimated, and divided into the object and reference arms. The object arm contains the sample, which is imaged by a microscope objective (MO_1; 5×/0.12) into a camera plane (CAM, UI 2280SE-M-GL, 2448×2048 square pixels, 3.45 μm pixel size) with a lateral magnification 8.6×.

Furthermore, two slightly tilted reference beams carrying the linear horizontal and linear vertical polarizations are generated at the output of the reference arm. The present microscope objectives MO_2 and MO_3 (both 5×/0.10) partially compensate for inherent phase curvature induced by the microscope objective MO_1. The reference and the object arms subsequently rejoin via a beam splitter (BS) placed before the camera. The formed hologram contains multiplexed information about the horizontal and vertical linear polarization components of the probed object. The spacing and orientation of the spatial carriers for the two reference beams are set to avoid crosstalk between the horizontally polarized component, vertically polarized component, and the zero order in the Fourier domain. Thus, demodulation of the multiplexed hologram provides each contribution independently. Further description of the setup can be found in [46,47].

The measurements were realized with the sample pipetted in a Petri dish. Then, two holographic snapshots of the same sample were taken. In one hologram, the object illumination was polarized diagonally, while anti-diagonally polarized illumination was set for the second snapshot hologram. Especially, three animal fibers were studied separately by this approach. As a result, several hundreds of hologram pairs for each fiber class were stored. Considering one fiber as one observation, we collected n_1=442 observations for class 1, n_2=221 for class 2, and n_3=396 for class 3. In the following paragraph, we detail the sample preparation and the DH reconstruction process.

2.2. Sample preparation

One sample of pure Cashmere (mean diameter = 15.56 μm, herein referred to as class 1) and two samples of Wool (mean diameter = 24.29, herein referred to as class 2 and 15.53 μm, herein referred to as class 3) are used. The purity of samples and fibers mean diameter are checked by SEM. Animal hair fibers samples are cut into snippets of 0.4 mm length by the microtome device, according to the IWTO 58–00 standard, before analysis.

Distilled water and absolute anhydrous ethanol were used for suspending the fibers (Carlo Erba, Italy). Firstly, the glassware adopted for making the suspensions was accurately washed with distilled water/ethanol 1:1 (v/v) solution and sonicated for 5 min in an ultrasonic bath

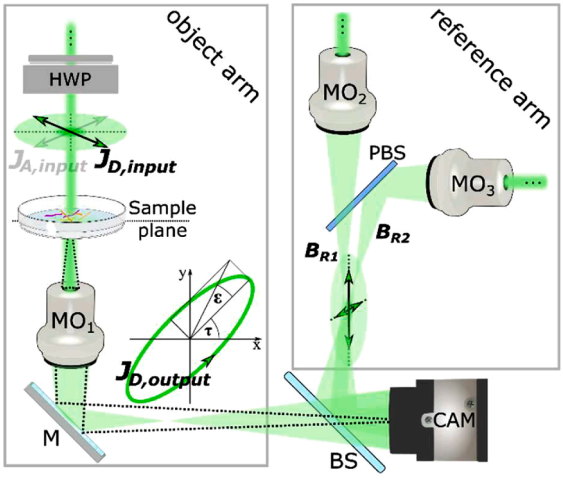

Fig. 1. Sketched polarization-sensitive DH setup. Half-wave plate (HWP), microscope objective (MO), mirror (M), beam splitter (BS), camera (CAM), polarizing beam splitter (PBS).

(Elma Transsonic T310). Secondly, the cleaned glassware was covered using aluminium foil. So, as suggested by Mossotti et al. [49], these two preliminary steps with minor modifications were done to avoid contamination of fibers present in the air. Glass containers were used for the sample suspensions. The cut fibers were suspended in 10 ml of distilled water. Then 5 ml of a 1:1 (v/v) distilled water/ethanol solution was added and the suspensions of the three different animal fibers were obtained. Specifically, two wool suspensions at a concentration of 0.15 % (w/w) and 0.19 % (w/w), as well as a cashmere suspension at a concentration of 0.07% (w/w) were prepared. The ethanol used in the preparation of suspensions allowed us to remove fibers that remained on the glass wall of the sample containers. Finally, the suspensions were strongly mixed for 5 min on a small shaker (IKA MS 3 basic) at 3000 rpm.

2.3. Polarization-sensitive DH principle

The polarization-resolved optical system allows observing the polarization state changes induced by the object. The hologram, H, produced by the interference between the arbitrarily polarized object beam, B_O, and two orthogonally polarized reference beams B_{R1} and B_{R2} can be expressed as:

$$H = |B_O + B_{R1} + B_{R2}|^2 = \left(|B_O|^2 + |B_{R1}|^2 + |B_{R2}|^2\right) + B_O(B_{R1}^* + B_{R2}^*) + \\ + B_O^*(B_{R1} + B_{R2}) \tag{1}$$

where the assumption of orthogonality $B_{R1}B_{R2}^* = B_{R1}^*B_{R2} = 0$ was used. The term $|B_O|^2 + |B_{R1}|^2 + |B_{R2}|^2$ represents the zeroth order of diffraction. When the reference beams B_{R1} and B_{R2} are polarized linearly horizontally and linearly vertically, the +1 diffraction orders $B_OB_{R1}^*$ and $B_OB_{R2}^*$ carry information of horizontal and vertical polarization components of B_O, respectively. Meanwhile, $B_O^*B_{R1}$ and $B_O^*B_{R2}$ are complex conjugated replicas. Hence, both valuable diffraction orders are separately filtered out and demodulated. The corresponding complex amplitudes are back-propagated to the object best-focus plane at distance d_F by applying the angular spectrum propagation method [50,51]. Thus, the horizontal (CW_1) and the vertical (CW_2) complex amplitudes of the object are recovered. Especially, the difference between the horizontal and vertical phase allows quantifying the birefringence-related features induced by the object [43].

In a more general approach, the polarization transformation induced by the probed object can be described by its Jones matrix, M [47,50-52]. The output Jones vector J_{output} after passing the sample can be expressed by the following formula:

$$J_{output} = MJ_{input} \tag{2}$$

where J_{input} represents polarization of the beam illuminating the object. Thus, when J_{input} is set and the J_{output} is measured, the Jones matrix M may be retrieved. Let D and A subscripts indicate diagonal and anti-diagonal linearly polarized beams. Hence, the assumed Jones vectors can be written in the form:

$$J_{D,input} = \frac{1}{\sqrt{2}}\begin{bmatrix}1\\1\end{bmatrix},\ J_{A,input} = \frac{1}{\sqrt{2}}\begin{bmatrix}1\\-1\end{bmatrix} \tag{3}$$

$$J_{D,output} = \begin{bmatrix}CW_{D1}\\CW_{D2}\end{bmatrix},\ J_{A,output} = \begin{bmatrix}CW_{A1}\\CW_{A2}\end{bmatrix} \tag{4}$$

After some calculations, considering Eq.2, the Jones matrix M is obtained as:

$$M = \begin{bmatrix}M_{11} & M_{21}\\M_{12} & M_{22}\end{bmatrix} = \frac{1}{\sqrt{2}}\begin{bmatrix}CW_{D1} + CW_{A1} & CW_{D1} - CW_{A1}\\CW_{D2} + CW_{A2} & CW_{D2} - CW_{A2}\end{bmatrix} \tag{5}$$

Consequently, the Jones matrix M, allows to analyze the eigenvectors (***EVs***) and eigenvalues (*EDs*) of the object. Because the ***EVs*** represent polarization ellipses they can be characterized by the major axis orientation angle τ and the ellipticity angle ε [46].

The used linearly polarized laser has a long coherence length (in order of tens of meters). The polarization state in the independent reference arms and the signal arm is finely set by polarizing beam splitters (extinct ratio 1:1000 according to the manufacturer). Indeed, calibration measurements presented in the recent article [53] demonstrated the correct Jones-matrix reconstruction over the whole considered field of view. Moreover, the presence of fully polarized light in the optical setup was proved in initial calibrations in the reference [46], where parameters of the output polarization ellipse were measured by a compensator-based technique. Such technique is based on detection of the sharp intensity extinction ('null-intensity'), which can be achieved only for fully polarized light. If the light was only partially polarized there would remain transmitted light reducing the visibility of the intensity extinctions, which was not observed during calibrations. In summary, the sharp null intensity detection and accurate Jones matrix reconstruction demonstrate that the light in the setup is fully polarized, with no significant depolarization.

2.4. Features analysis

To discriminate the three types of animal fibers, we considered the calculated amplitudes and phases of CW_{D1} and CW_{D2}. Then, five conventional morphological features have been directly extracted from the estimated object binary support, i.e., the diameter, the area, the major axis of the fiber shape, the eccentricity, and the orientation of the sample. Moreover, we extracted polarization parameters of EV_1 and EV_2, including the ellipticity angles ε_1, ε_2 and orientation angle τ_1 minus the local shape, and the orientation angle τ_2 minus the orthogonal local shape [46].

2.4.1. Jones features

For each textile fiber, the Jones matrix characteristics were used. From these parameters, 80 'Jones features' have been extracted. In particular, we calculated the mean value, the standard deviation, the median, the mode, the kurtosis, the skewness, the mean absolute deviation and the median absolute deviation of the inner product between eigenvectors ($|EV_1 \cdot EV_2|$), i.e., the degree of polarization homogeneity, the absolute value of the ratio between eigenvalues ($|\frac{ED_1}{ED_2}|$), i.e., the anisotropic absorption, the phase delay between eigenvalues ($\angle\frac{ED_1}{ED_2}$), the ellipticity angles (ε_1, ε_2) and the major axis orientation of the first eigenvector τ_1 minus the local shape, and the second eigenvector τ_2 minus the orthogonal local, real and imaginary parts of the ratio between eigenvalues (real($\frac{ED_1}{ED_2}$), imag($\frac{ED_1}{ED_2}$)), and the rescaled phase difference between eigenvalues ($\angle\frac{ED_1}{ED_2}\cdot\frac{\lambda}{2\pi m}$), where λ is the wavelength of the light source and m the minor-axis length of the fiber shape, i.e., the birefringence. An in-depth description of the physical meaning for these parameters is provided in [46].

2.4.2. Other polarization-based DH features

Considering the amplitude map $|CW_{D1}|$, phase $\angle CW_{D1}$ map, and mutual phase-difference map $\angle\frac{CW_{D1}}{CW_{D2}}$ of the textile fibers, the first order and the textural features have been extracted to study the image histogram properties and the gray-tone spatial dependencies [54-56].

Specifically, among the first order features: the mean value, the standard deviation, the interquartile range, the root mean square, the entropy, the skewness and the kurtosis have been evaluated for $|CW_{D1}|$, $\angle CW_{D1}$ and $\angle\frac{CW_{D1}}{CW_{D2}}$ maps of each sample involved in the measurements, reaching 21 features. The textural features used in this analysis are calculated from the gray level co-occurrence matrix (GLCM) [55] and the Gray Level Run Length Matrix (GLRLM) [56], totalizing 69 GLCM and 132 GLRLM. GLCM and GLRLM reveal how the pixel gray levels distribute in the neighborhood for a fixed image direction and the run of the pixel gray levels in different directions, respectively. The GLRLM is

analyzed changing the direction in 4 angles (0°, 45°, 90° and 135°).

A complete description of these features is reported in ref. [47].

2.4.3. Features balancing

The total number of features used in the classification process is the sum of the previously mentioned features, i.e., 307, schematized in Table1.

However, the dataset obtained from the measurements is not balanced due to a different number of samples of the three classes found during the experimental campaign. Class 1, class 2 and class 3 respectively have n_1=442, n_2=221 and n_3=396 samples. Of course, a proper machine learning analysis should be ideally performed on a balanced dataset. To fix the balancing issue, we applied the Synthetic Minority Oversampling Technique (SMOTE algorithm) [57] to synthetize the features of the minority classes until obtaining the same numerosity of samples of the majority class, i.e., 442. This technique selects a type of feature and randomly draws new class samples considering feature classes examples in the neighborhood. Each class has 442 samples, collecting 1326 samples for 307 different features.

2.4.4. Features importance

First, the whole dataset of features has been used for the classification task. However, a certain degree of redundancy is expected considering the correlation between e.g., the features extracted directly from the polarization channels readout and the Jones matrix features. Hence, two strategies of feature selection have been tested independently, which are expected to improve the classification performance [58]. Firstly, a channel-based selection is applied. The Minimum Redundancy and Maximum Relevance algorithm (MRMR) [59] is used for each channel. The MRMR selection orders the sets of features starting from the less redundant features that have the maximum power of prediction with respect to the labels. Thus, the MRMR algorithm assigns an 'importance weight' to each feature. The distribution plot of the 'importance weights' will decrease from left to right and will have a drop-in score that determines the features to select. Secondly, a PCA selection [60] is applied to the whole dataset.

2.5. Classification pipeline

The 3-class classification has been performed by means of the Matlab® Classification Learner tool that allowed us comparing the performance of different classifiers. We split the dataset into training and testing subsets with a partition of 70 % and 30 % respectively. A 10-fold cross-validation has been carried out [61]. We trained several families of classifiers and tested them three times, independently: using the whole set of features, using the channel-based MRMR selected subset of features, and using the feature subset selected by PCA.

The classifiers families are the Linear, the Discriminant, the Trees, the Naïve Bayes, the SVMs (Support Vector Machines) and the KNNs (k-Nearest Neighbors) [61,62]. Classification performance have been evaluated considering the validation accuracy of the training dataset through the k-folding test, the test accuracy, and the confusion matrices [62] calculated after classifying the testing dataset.

In addition, the performance of binary classification tasks has been evaluated. In other words, we considered the case in which one needs to discriminate only class 1 vs. class2, class 1 vs. class 3 or class 2 vs. class 3. These cases can be relevant in industry practice when there is a hypothesis for a certain textile composition that needs to be confirmed or denied by quality assessments. We carried out the features selection and performance evaluation similarly to the 3-class discrimination task.

Table 1
Polarization-based DH features scheme.

Channels	First order	GLCM features	GLRLM features
$\lvert CW_{D1}\rvert$ amplitude map	7	23	44
$\angle CW_{D1}$ phase map	7	23	44
$\angle \frac{CW_{D1}}{CW_{D2}}$ phase map	7	23	44
Morphological features	5		
Jones features	80		
Total features	307		

3. Results and discussions

As previously discussed, quality assessments require a visual microscopy approach to distinguish different types of animal hair fibers and quantify their amount by naked-eye counting, which is a cumbersome and time-consuming process. The features to which experienced operators pay attention are usually the morphological ones, such as the diameter; besides, the surface roughness may characterize them when observed under light microscopes [13-22]. However, some animal fibers have similar distributions of shape or roughness parameters, and their identification becomes prone to errors. To overcome limitations and automatize the discrimination process, thus fastening the analysis, here we prove that the use of a polarization-sensitive DH system adds enough information channels to help discriminating animal fibers.

We acquired and reconstructed several polarization-multiplexed holograms of the three classes in a Petri dish, as was described previously. In particular, we measured each class alone in order to obtain a labelled dataset for training purposes. In principle, a first trivial clustering of the three types could be performed relying on the mere diameter of the microfiber. A bar-plot of the diameter for the three classes is shown in Fig. 2. Class 2 has a larger median value than the medians of the other two classes. However, the large standard deviation implies a non-negligible overlap with the other classes, i.e., numerous fibers belonging to class 2 have diameters comparable to the typical diameters of the other two classes. Besides, class 1 and class 3 mostly overlap and cannot be trivially clustered. This means that a robust analysis based on the sole diameter is unfeasible. Similar considerations could be made analyzing the other morphological features.

This morphological interclass homogeneity is the main responsible factor for misclassifications occurring when mere morphological inspections are carried out under the optical microscope.

To enforce the classification analysis, we added the polarization-based features to the morphological descriptors. In particular, for each class the 2D maps of the major axis orientation angles τ_1,τ_2 and the ellipticity angles ε_1,$\varepsilon_2$were calculated for both eigen-polarizations EV_1 and EV_2 (Fig. 3), respectively.

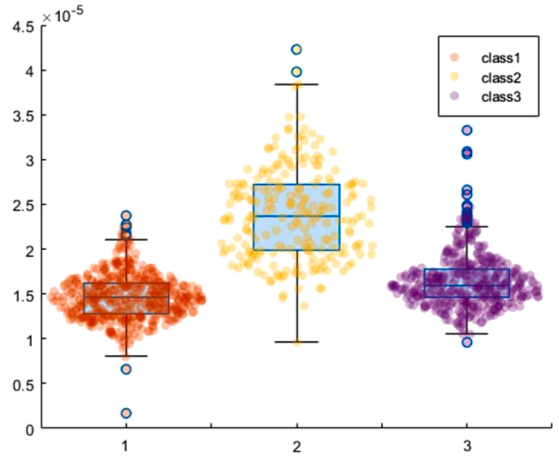

Fig. 2. Diameters boxplot. The 3 classes of animal fibers have been plotted with respect to their diameter. The line of the boxplot stands for the median of the diameters, and the bars indicate the standard deviation. The blue circles are the outliers. (For interpretation of the references to color in this figure legend, the reader is referred to the web version of this article.)

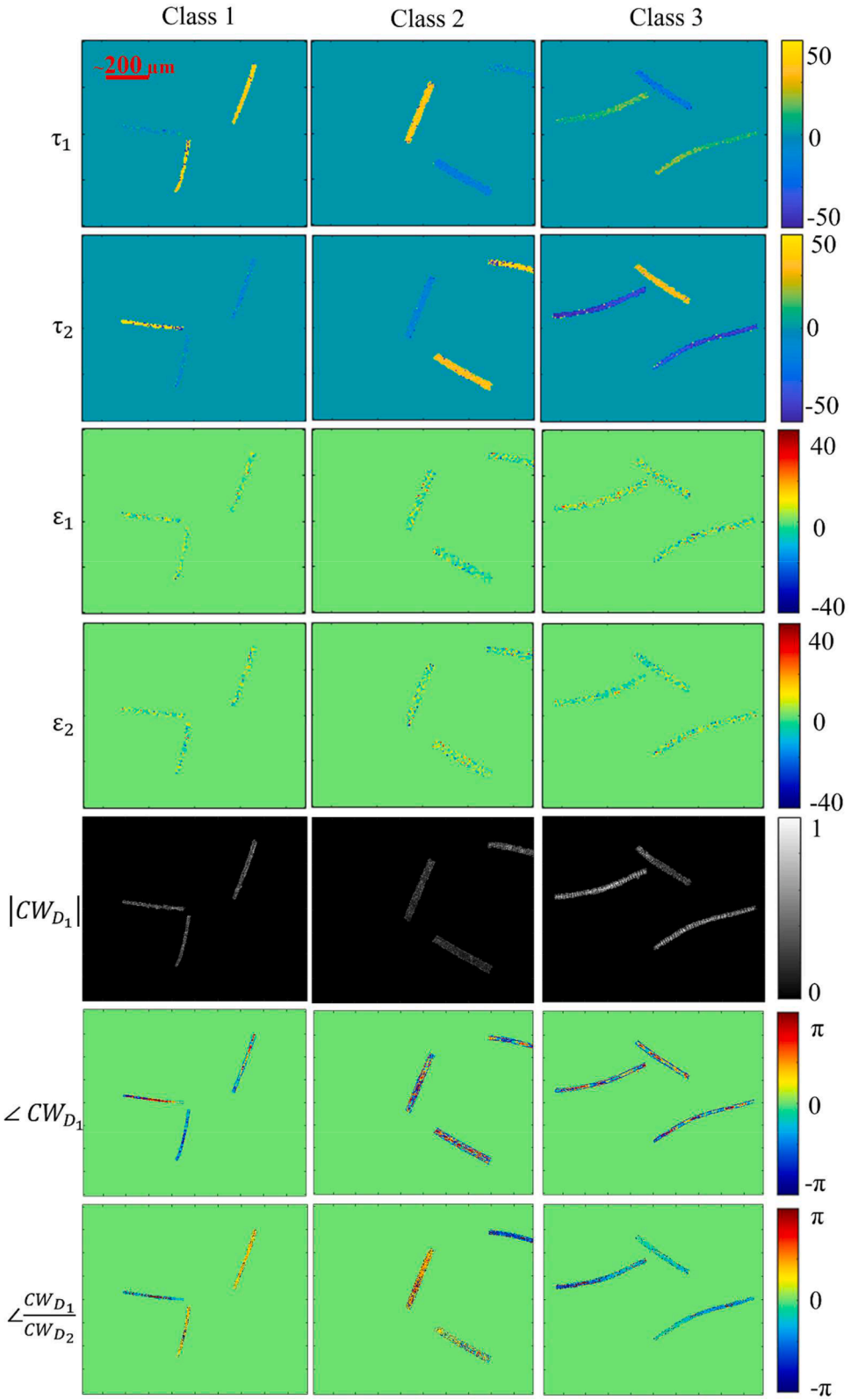

Fig. 3. Polarization-sensitive DH channels for the three types of wool microfibers. The Jones formalism allowed to evaluate the major axis orientation angles (τ_1, and τ_2) and the ellipticity angles (ε_1 and ε_2) of both eigenvectors. The amplitude and phase-difference maps are the images with the $|CW_{D1}|$, $\angle CW_{D1}$, and $\angle \frac{CW_{D1}}{CW_{D2}}$ notations.

Moreover, inspection of the $|CW_{D1}|$, $\angle CW_{D1}$ and $\angle \frac{CW_{D1}}{CW_{D2}}$ maps for each class suggests these information channels could gather additional interclass diversity, which is in principle useful for classification scopes. Jones matrix features and the other polarization-based holographic features are extracted according to a previous text.

The PCA was performed on the 307 features dataset. The first three principal components are scattered in the plot in Fig. 4 to confirm the features tendence to cluster with respect to the class labels. The 3 PCA components in the 3D scatter plot do not cluster well the 3 classes,

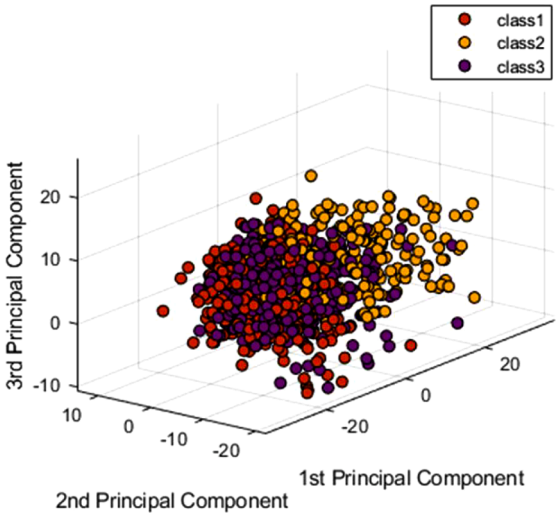

Fig. 4. PCA plot on all extracted features. The PCA algorithm is applied on the whole dataset acquired. The first 3 principal components in the 3D scatter plot show the features weak capability of clustering the animal fibers.

meaning that this preliminary approach is not the most appropriate or a robust classification.

Moreover, the PCA in Fig. 4 describes the complexity of the classification problem, which cannot be trivially handled by multi-parameter clustering. For this reason, we adopted a machine learning approach.

To empower the training step, the whole features dataset was balanced as described in *Section 2.4.3*. After partitioning the training and test subsets (70% vs 30 %), the training set was uploaded in the Classification Learner tool [61] to train all the classifiers. We used a 10-fold cross-validation to assess and compare the performance of the classifier models. The highest validation accuracy determined the classifier to test for the 3-class classification task, which was the 89.3 % of the quadratic SVM [61]. The test accuracy was 85.9 % and the confusion matrix of the test is reported in Fig. 5.

Of course, redundancy is expected considering the large number of features involved and the correlation between them according to the formulation in Section 2.

The features selection adopted in this work is the MRMR algorithm that eliminates the redundancy and enhances the most important features. We applied the MRMR algorithm to the different feature subsets, i.e., morphological, Jones features, $|CW_{D1}|$ features, $\angle CW_{D1}$ features and $\angle \frac{CW_{D1}}{CW_{D2}}$ features, resulting in a supervised cluster selection. In Table S1 of the Supplementary Information, the 22 selected descriptors are summarized.

The MRMR selected dataset underwent the machine learning pipeline applied for the whole dataset. The Cubic SVM has shown the highest validation accuracy, i.e., 82.5 %, reaching a test accuracy of 82.6 %. The new accuracies are lower than the accuracies obtained with the entire features dataset. Thus, the MRMR selection did not improve the classification performance, meaning that the used selection approach is not suitable for the dataset under analysis. Therefore, a PCA selection with an explained variance of 95 % [61] has been enabled on the Classification Learner tool before starting the training. The tool considered the first 33 principal components as selected features.

The best classifier in this case was the Fine Gaussian SVM that reached a validation accuracy of 89.1 % and a test accuracy of 89.4 %. The PCA selection achieved better results in terms of accuracy. In Fig. 5, the confusion matrices show other performance metrics for all classes, such as the Predictive Positive Values (PPV), the False Discovery Rate (FDR), the true positive rate (TPR) and the false negative rate (FNR) [61].

Comparing the PPV percentages of the MRMR selected dataset with

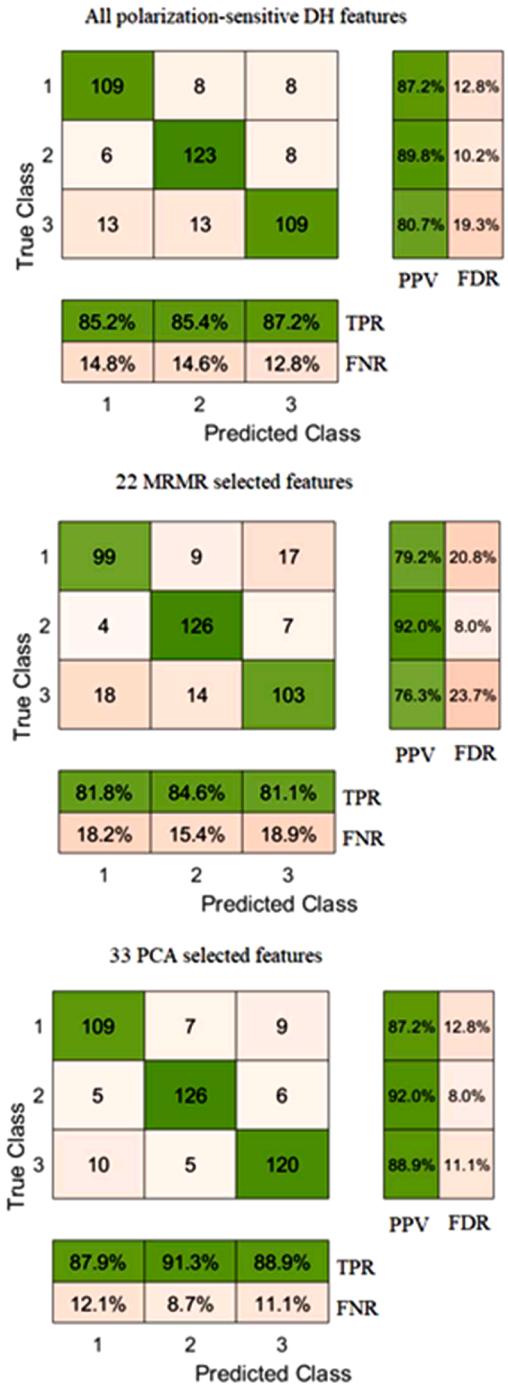

Fig. 5. Confusion matrices for the three-class discrimination task. The central matrix is the number of the occurrences of the true classes with respect to the predicted classes. The row summary reports the TPR and the opposite FNR. The column summary reports the PPV and the FDR [54].

the whole dataset of features, the PPV of class 2 is higher in the MRMR classification than in the whole features classification, i.e., 92% vs 89.8 %, meaning that the MRMR selection is more precise for class 2 discrimination. However, the MRMR selected dataset furnishes the lowest PPV percentages for class 1 and class 3. The highest PPV and TPR percentages result from the PCA selected dataset, around the 90 %.

Noteworthy, to train a classifier, we first imaged the single fibers belonging to the three classes alone. In this way the classifier learns the regions of decision and the values of the features to be associated with each single class. Then, as in typical machine learning problems, the

Table 2
Binary classifications results.

Classes	Best classifier	Val acc	Test acc	PPV	TPR
	All 307 features				
Class1 vs Class2	Quadratic SVM	93.4 %	93.2 %	95.9 % vs 95.1 %	94.4 % vs 96.4 %
Class 1 vs Class3	Quadratic SVM	96.0 %	95.5 %	91.1 % vs 95.1 %	90.2 % vs 91.5 %
Class2 vs Class3	Cubic SVM	92.9 %	90.9 %	90.2 % vs 91.5 %	90.2 % vs 91.5 %
	22 MRMR selected features				
Class 1 vs Class 2	Cubic SVM	94.0 %	93.6 %	95.9 % vs 91.5 %	90.8 % vs 96.3 %
Class 1 vs Class 3	Quadratic SVM	85.3 %	88.3 %	88.6 % vs 88.0 %	86.5 % vs 89.9 %
Class 2 vs Class 3	Cubic SVM	91.0 %	87.9 %	88.6 % vs 87.3 %	85.8 % vs 89.9 %
	PCA selected features (31 features for class1/class2; 34 for class1/class3 and 30 for class2/class3)				
Class 1 vs Class 2	Cubic SVM	94.8 %	94.0 %	92.7 % vs 95.1 %	94.2 % vs 93.8 %
Class 1 vs Class 3	Quadratic SVM	92.2 %	94.3 %	93.5 % vs 95.1 %	94.3 % vs 94.4 %
Class 2 vs Class 3	Fine Gaussian SVM	92.2 %	92.5 %	88.6 % vs 95.8 %	88.6 % vs 90.7 %

validation experiment is carried out to assess the classification performance. After this step, a testing experiment was blindly executed on the random single fiber (unknown by the classifier). Since the system images and judges each single microfiber alone, from the classifier standpoint there is no difference in having the sample physically mixed in the Petri dish (e.g. standard wool in cashmere yarn) or not (i.e. each population separately acquired). In our case, all the elements fall under the microscope eye and are classified, thus the two cases coincide.

In summary, reported results are very promising for automatic and accurate discrimination of animal hair fibers. In particular, the PCA-selected features set (33 principal components) outperformed the others using a fine gaussian SVM classifier. We adopted the machine learning pipeline applied in the 3-class classification case. Hence, for all classes combinations, the results of the binary classification with all 307 DH features, the binary classification with the 22 MRMR-selected features and the binary classification with the PCA-selected features are reported in Table 2. In particular, the binary classifications in Table 2 show high accuracies especially in discerning between class 1 and class 3, reaching a 96 % validation accuracy with a quadratic SVM trained on all 307 extracted features. The best classifier for the binary classification of class 1 vs. class 2 is the cubic SVM with a 94.8 % validation accuracy using the PCA selected dataset (31 features), while class 2 is better classified against class 3 using all features in a cubic SVM, reaching a 92.9 % validation accuracy.

Here, it's pertinent to discuss potential drawbacks of our method. Enhancing the robustness of our analyses would necessitate a larger pool of wool and cashmere samples, eliminating the need for dataset balancing algorithms like the SMOTE algorithm. This will be an essential step to validate the results across different datasets and conditions in order to ensure its generalizability and robustness in industrial applications. Factors such as variations in sample surface roughness and fibers stress/bending could affect the polarization state of light passing through the sample, leading to potential inaccuracies in measurements. Another drawback is the system throughput. We performed in Petri measurements and for each sample the Jones formalism needs two acquisitions, i.e. diagonal and anti-diagonal, to extract the Jones parameters. In future work, we aim to adopt polarization-sensitive DH in continuous flow to significantly increase throughput. Achieving single-shot polarization-sensitive DH acquisition is desirable for this purpose. One approach is to add an additional object arm to the interferometer to probe the sample simultaneously with diagonal and anti-diagonal linear polarizations, as demonstrated in ref. [63]. Another possibility is to use a polarization CMOS camera, as described in ref. [64]. Within manufacturing contexts, the integration of PS-DH microscopy into quality control procedures can be useful to uphold the authenticity and purity of cashmere products. This technology can provide precise differentiation between cashmere and wool fibers, thereby ensuring compliance with desired quality standards and deterring fraudulent activities associated with fiber blending. So far, these controls are outsourced to research labs where experts analyze each single fiber using microscopic techniques (light optical microscopy and scanning electron microscopy). This procedure is very slow, cumbersome, and subject to human errors. Above all, it depends on the experience and skills of the person called to analyze and distinguish the fibers. To assess the quality of a garment, at least 600 fibers should be analyzed from almost three samples taken from the textile materials. This procedure requires long time of analysis with high costs and few samples (not more than 2) can be processed in a day of work. To implement our new approach in industrial environment, an effort in system miniaturization and/or simplification should be done. The use of the recently introduced polarimetric CMOS camera will be an important step in this direction [64]. Also, the throughput should be increased to significantly improve the number of elements that can be judged in an industrial environment where timing is an essential requisite.

4. Conclusions

The need of textile industries of verifying the quality of garments, especially of cashmere products, has led the scientific community of textile sector not only to find objective, accurate and reliable methods of animal fibers discrimination, but also to try to automatize and fasten the identification process. Here, we applied a polarization-sensitive DH microscope in multiplexed configuration to optically characterize the animal hair fibers and the way they change the polarization states of the light probe. We analyzed the complete dataset of polarization-based DH features, originating from the birefringence of animal fibers and the eigen decomposition of their Jones matrix, which represented an additional value to the classical morphological features. The developed machine learning pipeline helped in classifying the 3 classes of fibers with high accuracy. In particular, the 33 PCA-selected features set reached a validation accuracy of 89.1 % training a Fine Gaussian SVM classifier, with PPV percentages of 87.2 %, 92 % and 88.9 % of class 1, class 2, and class 3, respectively.

For the binary classification task, validation accuracy higher than 93 % is reached using all 307 polarization-sensitive DH features to train quadratic and cubic SVM classifiers.

It's worth noting that the present study tackled a more complex and challenging problem compared to the work reported in ref. [39] where the Jones matrix formalism was sufficient to identify four different microplastic fibers and two natural ones in static recording mode, without the need of a machine learning implementation. Indeed, wool and cashmere fibers are much more similar each-others and the analysis of the feature's space is not enough to distinguish the three classes analyzed by simple clustering operations. This aspect is apparent from the PCA analysis in Fig. 4. In order to achieve all-optical identification between cashmere and wool we needed to add complexity in respect to the previous study. The results obtained in the present work are promising in terms of accuracy and reliability. Moreover, the use of pre-trained classifiers fastens the identification process, automatically contributing to the animal hair fibers quality check. A further future implementation would be the use of a more-complex imaging apparatus where the simultaneous recording of diagonal and antidiagonal illuminations will be possible, thus implementing the analysis on flowing samples at the aim to improve the throughput of the technology. Such improvement would realistically open to the industrial use of polarization sensitive DH for garment quality test, applicable also in the end-of-life textile materials recycling process.

CRediT authorship contribution statement

M. Valentino: Software, Validation, Writing – original draft. **J. Behal:** Methodology, Formal analysis, Investigation, Writing – original draft. **C. Tonetti:** Resources, Methodology, Writing – review & editing. **R.A. Carletto:** Investigation. **S. Itri:** Investigation. **P. Memmolo:** Software, Validation, Formal analysis. **E. Stella:** Methodology, Writing – review & editing. **L. Miccio:** Conceptualization, Methodology, Writing – review & editing, Supervision. **V. Bianco:** Conceptualization, Software, Writing – review & editing, Supervision. **P. Ferraro:** Conceptualization, Methodology, Writing – review & editing, Supervision.

Declaration of competing interest

The authors declare that they have no known competing financial interests or personal relationships that could have appeared to influence the work reported in this paper.

Data availability

Data will be made available on request.

Supplementary materials

Supplementary material associated with this article can be found, in the online version, at doi:10.1016/j.optlaseng.2024.108395.

References

[1] Kadolph SJ, Langford AL. Textiles, 9e. Upper Saddle River, NJ: Pearson Education; 2002.
[2] Markova I. Textile fiber microscopy: a practical approach. John Wiley & Sons Ltd; 2019.
[3] Wortmann FJ, Wortmann G, McCarthy B. Cashmere/yak blends: a vexing analytical problem. Wool Rec 2007;166(3750):33.
[4] McGregor B. Properties, processing and performance of rare natural animal fibres: a review and interpretation of existing research results. Rural Industries Research and Development Corporation; 2012. ISBN 978-1-74254-333-8.
[5] Hunter L, Mandela N. Mohair, cashmere and other animal hair fibres. Handbook of natural fibres, types, properties and factors affecting breeding and cultivation. 2012. p. 196–290. 1.
[6] Wildman AB. The microscopy of textile fibers. Wool Industries Research Association, Lund Humphries; 1954.
[7] Tortola PG. Understanding textiles. Macmillan Publishing Company; 1992. p. 4e.
[8] https://euipo.europa.eu/tunnel-web/secure/webdav/guest/document_library/observatory/documents/reports/trends_in_trade_in_counterfeit_and_pirated_goods/trends_in_trade_in_counterfeit_and_pirated_goods_en.pdf.
[9] Baloyi R, et al. Recent advances in recycling technologies for waste textile fabrics: a review. Text Res J 2024;94(3–4):508–29.
[10] Johnson I, Cohen AC, Sarkar AKJJ. Pizzuto's fabric science. Bloomsbury Publishing; 2015. p. 11e.
[11] Zoccola M, Bhavsar P, Anceschi A, Patrucco A. Analytical methods for the identification and quantitative determination of wool and fine animal fibers: a review. Fibers 2023;11:67. https://doi.org/10.3390/fib11080067.
[12] Phan KH, Wortmann FJ, Wortman G, Arns W. Characterization of specialty fibers by scanning electron microscopy. In: Proceedings from 1st international symposium on specialty animal fibers. 103. Aachen. Schrift. der Deutsches Wollforschungsinstitutet; 1988. p. 137–62.
[13] Greaves PH, Saville BP. Microscopy of textile fibres: microscopy handbook 32. Oxford: Royal Microscopical Society, BIOS Scientific Publications; 1995.
[14] Wortmann FJ, Wortmann G, Roes J. Light microscopy of yak and cashmere fibre blends. In: Proc. 2nd inter. symp. speciality animal fibers. 106. Aachen. Schrift. der Deutsches Wollforschungsinstitutet; 1990. p. 104–12.
[15] Wortmann FJ, Arns W. Quantitative fiber mixture analysis by scanning electron microscopy. Text Res J 1986;56:442–6.
[16] Vineis C, Tonetti C, Paolella S, et al. A UPLC/ESI–MS method for identifying wool, cashmere and yak fibres. Text Res J 2014;84(9):953–8.
[17] Wortmann FJ. SEM-analysis of wool/specialty fibre blends - state of the art. In: Proc. 2nd inter. symp. speciality animal fibers. 106. Aachen. Schrift. der Deutsches Wollforschungsinstitutet; 1990. p. 113–20.
[18] Zhu Y, Jiayi H, Li Y, Li W. Image identification of cashmere and wool fibers based on the improved Xception network. J King Saud Univ 2022;34:9301–10.
[19] Wortmann G, Wortmann FJ. Wool contamination in cashmere. In: Proc. 2nd inter. symp. speciality animal fibers. 106. Aachen. Schrift. der Deutsches Wollforschungsinstitutet; 1990. p. 138–46.
[20] Phan KH, Rutten S, Popescu C. Yak and Sheep's wool: the fibres hidden behind cashmere. In: Proc. 4th inter. cashmere determination technique symp. China: China National Cashmere Products Engineering and Technical Centre and China Inner Mongolia Erdos Cashmere Group Corporation; 2008. p. 49–59.
[21] Javkhlantugs N, Ankhbayar E, Tegshjargal K, Enkhjargal D, Ganzorig C. AFM study of untreated and treated fibers of Mongolian cashmere. Mater Sci Forum 2009;610-613:175–8.
[22] Bergfjord C, Holst B. A procedure for identifying textile bast fibers using microscopy: flax, nettle/ramie, hemp and jute. Ultramicroscopy 2010;110:1192–7.
[23] Quantitative analysis of cashmere, wool, other specialty animal fibres and their blends. UNI EN ISO 17751-12:2016.
[24] Scanning electron microscopic analysis of speciality fibres and sheep's wool and their blends. IWTO-58-00.
[25] Tonetti C, Vineis C, Aluigi A, Tonin C. Immunological method for the identification of animal hair fibres. Text Res J 2012;82(8):766–72.
[26] Sagar AJG, Calvert E, McCarty BJ. Characterisation of keratin fibres by chemical analysis. In: Proceedings of the 2nd international symposium on speciality animal fibres; 1990. p. 147–64.
[27] Rivett D, Logan R, Tucker DJ, Hudson AHF. The lipid composition of animal fibres. In: Proceedings of the 1st international symposium on speciality animal fibres; 1988. p. 128–36.
[28] Paolella S, Bencivenni M, Lambertini F, Prandi B, Faccini A, Vineis C, Tonetti C, Sforza S. Identification and quantification of different species in animal fibres by LC/ESI-MS analysis of keratin-derived proteolytic peptides. J Mass Spectrom 2013;48(8):919–26.
[29] Vineis C, Tonetti C, Paolella S, Pozzo P, Sforza S. A UPLC/ESI–MS method for identifying wool, cashmere and yak fibres. Text Res J 2014;84(9):953–8.
[30] Vineis C, Tonetti C, Sanchez Ramirez DO, Carletto RA, Varesano A. Validation of UPLC/ESI-MS method used for the identification and quantification of wool, cashmere and yak fibres. J Text Inst 2017;180:2180.

[31] Fei J, Liu M, Zhang S, Chen X, Zhang S. Technical note: a protein analysis-based method for identifying Shahtoosh. Forensic Sci Int 2022;336:111341.
[32] Tonetti C, Varesano A, Vineis C, et al. Differential scanning calorimetry for the identification of animal hair fibres. J Therm Anal Calorim 2015;119:1445–51.
[33] Penner MH. Basic principles of spectroscopy. In: Nielsen SS, editor. Food analysis. Food science text series. Cham: Springer; 2017.
[34] McGregor BA, Liu X, Wang XG. Comparisons of the Fourier transform infrared spectra of cashmere, guard hair, wool and other animal fibres. J Text Inst 2018; 109:813–22.
[35] Vinichenko SN, Ryzhkova EA, Nikonov MV. Use of infrared spectroscopy for valuating the quality of fiber mixing. Fibre Chem 2019;51(1).
[36] Notayi M, Hunter L, Engelbrecht JA, Botha AF, Minnaar EG, Lee ME, Erasmus R. The application of Raman spectroscopic ratiometric analysis for distinguishing between wool and mohair. J Nat Fibers 2022;19:11536–46.
[37] Sun X, Yuan H, Song C, Li X, Hu A, Yu S, Ren Z. A novel drying-free identification method of cashmere textiles by NIR spectroscopy combined with an adaptive representation learning classification method. Microchem J 2019;149:104018.
[38] Canaza-Cayo W, Alomar D, Quispe E. Prediction of alpaca fibre quality by near-infrared reflectance spectroscopy. Animal 2013;7:1219–25.
[39] Peets P, Kaupmees K, Vahur S, et al. Reflectance FT-IR spectroscopy as a viable option for textile fiber identification. Herit Sci 2019;7:93.
[40] Kim MK. Principles and techniques of digital holographic microscopy. SPIE Rev 2010;1.
[41] Popescu G, Ikeda T, Dasari RR, Feld MS. Diffraction phase microscopy for quantifying cell structure and dynamics. Opt Lett 2006;31:775–7.
[42] Colomb T, Dahlgren P, Beghuin D, Cuche E. Polarization imaging by use of digital holography. Appl Opt 2002;41:27–37.
[43] Colomb T, Dürr F, Cuche E, Marquet P, Limberger HG, Salathé RP, Depeursinge C. Polarization microscopy by use of digital holography: application to optical-fiber birefringence measurements. Appl Opt 2005;(21):44.
[44] Shribak M, Oldenbourg R. Techniques for fast and sensitive measurements of two-dimensional birefringence distributions. Appl Opt 2003;42:3009–17.
[45] Sierra I, Chialanza MR, Faccio R, Carrizo D, Fornaro L, Pérez-Parada A. Identification of microplastics in wastewater samples by means of polarized light optical microscopy. Environ Sci Pollut Res 2020;27:7409–19.
[46] Běhal J, Valentino M, Miccio L, et al. Toward an all-optical fingerprint of synthetic and natural microplastic fibers by polarization-sensitive holographic microscopy. ACS Photonics 2022;9(2):694–705.
[47] Valentino M, Běhal J, Bianco V, et al. Intelligent polarization-sensitive holographic flow-cytometer: towards specificity in classifying natural and microplastic fibers. Sci Total Environ 2022;815:152708.
[48] Yang Y, Huang H-Y, Guo C-S. Polarization holographic microscope slide for birefringence imaging of anisotropic samples in microfluidics. Opt Express 2020; 28:14762–73.
[49] Mossotti R, Dalla Fontana G, Anceschi A, Gasparin E, Battistini T. Preparation and analysis of standards containing microfilaments/microplastic with fibre shape. Chemosphere 2021;270:129410.
[50] Jones RC. A new calculus for the treatment of optical systems. J Opt Soc Am 1941; 31:488–93.
[51] Colomb T, Cuche E, Montfort F, Marquet P. Jones vector imaging by use of digital holography: simulation and experimentation. Opt Commun 2004;231:137–47.
[52] Goodman JW. Introduction to Fourier optics. McGraw-Hill; 1996.
[53] Coppola S, Vespini V, Běhal J, Bianco V, Miccio L, Grilli S, De Sio L, Ferraro P. Drop-on-demand pyro-electrohydrodynamic printing of nematic liquid crystal microlenses. ACS Appl Mater Interfaces 2024;16(15):19453–62.
[54] Zwanenburg A, Vallières M, Löck S, Leger S, et al. Image biomarkerstandardisation initiative: standardized quantitative radiomics for high-throughput image-based phenotyping. Radiology 2020;295:328–38.
[55] Haralick RM, Shanmugam K, Dinstein I. Textural features for image classification. IEEE Trans Syst Man Cybern 1973;SMC-3(6):610–21.
[56] Galloway MM. Texture analysis using gray level run lengths. Comput Graph Image Process 1975;4(2):172–9.
[57] Chawla NV, Bowyer KW, Hall LO, Kegelmeyer WP. SMOTE: synthetic minority over-sampling technique. J Artif Intell Res 2002;16:321–57.
[58] Kira K, Rendell LA. The feature selection problem: traditional methods and new algorithm. In: AAAI-92 computer science; 1992.
[59] Radovic M, Ghalwash M, Filipovic N, et al. Minimum redundancy maximum relevance feature selection approach for temporal gene expression data. BMC Bioinformatics 2017;18:9.
[60] Song F, Guo Z, Mei D. Feature selection using principal component analysis. In: International conference on system science, engineering design and manufacturing informatization; 2010. p. 27–30.
[61] MathWorks: https://it.mathworks.com/help/stats/choose-a-classifier.html#bunt0ky, last Accessed 15 June 2023.
[62] Bishop CM. Pattern recognition and machine learning. Springer Verlag New York; 2006.
[63] Yue Q-Y, Cheng Z-J, Han L, Yang Y, Guo C-S. One-shot time-resolved holographic polarization microscopy for imaging laser-induced ultrafast phenomena. Opt Express 2017;25:14182–91. https://doi.org/10.1364/OE.25.014182.
[64] Li Y, Zhu Y, Huang J, et al. High-throughput microplastic assessment using polarization holographic imaging. Sci Rep 2024;14:2355. https://doi.org/10.1038/s41598-024-52762-5.